Journal of
Materials Chemistry A

Accepted Manuscript

This is an *Accepted Manuscript*, which has been through the RSC Publishing peer review process and has been accepted for publication.

Accepted Manuscripts are published online shortly after acceptance, which is prior to technical editing, formatting and proof reading. This free service from RSC Publishing allows authors to make their results available to the community, in citable form, before publication of the edited article. This *Accepted Manuscript* will be replaced by the edited and formatted *Advance Article* as soon as this is available.

To cite this manuscript please use its permanent Digital Object Identifier (DOI®), which is identical for all formats of publication.

More information about *Accepted Manuscripts* can be found in the **Information for Authors**.

Please note that technical editing may introduce minor changes to the text and/or graphics contained in the manuscript submitted by the author(s) which may alter content, and that the standard **Terms & Conditions** and the **ethical guidelines** that apply to the journal are still applicable. In no event shall the RSC be held responsible for any errors or omissions in these *Accepted Manuscript* manuscripts or any consequences arising from the use of any information contained in them.

Journal of Materials Chemistry A RSCPublishing

ARTICLE

Effect of iron-carbide formation on the number of active sites in Fe-N-C catalysts for the oxygen reduction reaction in acidic media

Cite this: DOI: 10.1039/xoxxoooooox

Received ooth January 2012,
Accepted ooth January 2012

DOI: 10.1039/xoxxoooooox

www.rsc.org/

Ulrike I. Kramm,[a,b] Iris Herrmann-Geppert,[a] Sebastian Fiechter,[a] Gerald Zehl,[a] Ivo Zizak,[c] Iris Dorbandt,[a] Dieter Schmeißer,[b] and Peter Bogdanoff[a]

In this work Fe-N-C catalysts were prepared by the oxalate-supported pyrolysis of FeTMPPCl or H_2TMPP either in the presence or absence of sulfur during the pyrolysis process. The well-known enhancing effect of sulfur-addition on the oxygen reduction activity was confirmed for these porphyrin precursors. The pyrolysis process was monitored in-situ by high-temperature X-ray diffraction under synchrotron radiation (HT-XRD) and thermogravimetry coupled with mass-spectroscopy (TG-MS). It was found that the beneficial effect of sulfur could be attributed to the prevention of iron-carbide formation during the heat-treatment process. In case of pyrolysis of the sulfur-free precursors an excessive iron-carbide formation leads to a disintegration of FeN_4-centers; hence, limiting the number of ORR active sites on the final catalyst. Physical characterization of the catalysts by bulk elemental analysis, X-ray diffraction (XRD), Raman and ^{57}Fe Mößbauer spectroscopy confirmed the outcome from HT-XRD and TG-MS. It could be shown, that the avoidance of carbide formation during pyrolysis represents a promising way to enhancing the density of ORR active sites on those catalysts. This can be done either by sulfur-addition or the performance of an intermediate acid-leaching. As iron carbide is often found as by-product in the preparation of Fe-N-C catalysts this work gives some general strategies for enhancing the density of active sites enabling higher current densities.

Introduction

For automotive application the utilization of Polymer-Electrolyte-Membrane Fuel Cells (PEM-FC) as power source is one of the most promising techniques especially in sparsely populated areas of e.g. North America. State-of-the-art catalysts are carbon-supported platinum (Pt/C) or its alloys. While platinum is an excellent catalyst for the hydrogen oxidation reaction (HOR) it reveals only a sluggish performance for the oxygen reduction reaction (ORR). Therefore, most of the platinum in today's fuel cells is used on the cathode, in order to get the reaction run.

However, for economic reasons catalyst costs have to be reduced as they contribute by 33 % to the overall costs of a FC stack.[1] Most effective would be the replacement of platinum by cheap non-noble metal catalysts (NNMC). The most promising alternative are the so-called Fe-N-C catalysts. Recent results demonstrate that these catalysts can indeed compete against platinum in terms of ORR activity, while their long-term performance has still be improved.[2-4]

The oxalate-supported pyrolysis has proven to be quite effective in the preparation of Me-N-C catalysts.[5-10] Especially in terms of active site density this technique is beneficial as no additional carbon support is required.[5] In previous work we demonstrated that (i) different oxalates[6] and (ii) different porphyrins can be utilized in this preparation.[10,11] The achievable activity depends on the optimized combination of both. The two most important steps in improving the ORR activity of these catalysts were the findings that much higher current densities are reached when sulfur is added to the precursor mixture of porphyrin plus iron oxalate [7,12] and that a second heat-treatment can drastically enhance the ORR activity.[8,9,11]

The performance of this second heat-treatment in different gas atmospheres enabled the preparation of catalysts with different ORR activity and various concentrations of iron species as determined by ^{57}Fe Mößbauer spectroscopy.[8] This approach enabled a direct correlation between one specific FeN_4-center and the ORR activity. In a recent publication we have shown that the turn-over frequency related to this active site depends on the electron density on the iron center.[13] It can be tuned for instance, by a change of the pyrolysis temperature.

Regarding the amount of sulfur to be added, the ratio of sulfur to iron has to be optimized as undersized ratios might not enable optimal improvement while an oversized sulfur quantity will cause the formation of FeS_x ($x > 1$) type phases with poor solubility in acidic medium.[14] For example, although acid-leached at boiling temperature, the so called PANI-Fe-C catalysts exhibit large concentrations of Fe_3S_4 which can be explained by the reaction of ammonium peroxidisulfate (APS) residuals (from the polymerization step) with the iron source.[15] A beneficial effect of sulfur on ORR activity of Me-N-C catalysts was also described by Contamin et al. and Hatchard et al..[16,17]

Catalysts prepared by the oxalate-supported pyrolysis under sulfur-addition exhibited the best performance in RDE experiments in a cross-laboratory comparison of different institutes worldwide.[18] In

this publication the activity was enhanced by a multi-step preparation. After the first heat-treatment in inert gas followed by an acid-leaching, a second heat-treatment in forming gas with subsequent acid-leaching and a third heat-treatment in CO_2 were applied.[18]
The catalysts discussed in this work were also prepared by the oxalate-supported pyrolysis, but characterized just after the first heat-treatment plus acid-leaching. This is because the focus of this work was not to beat all previous results with respect to ORR activity, but to elucidate the reason for the different performance of catalysts prepared by this technique with and without sulfur-addition to the precursor mixture.

Experimental

I. Preparation of Fe-N-C catalysts

Precursor preparation (± S) In order to prepare a sulfur-free precursor, 1.3 mmol FeTMPPCl (TriPorTech, 95 % purity) was mixed with 28.6 mmol iron-oxalate dihydrate (Riedel de Häen) in a mortar until a homogeneous precursor mixture was obtained. To prepare a sulfur-containing precursor 1.2 mmol sulfur (S_8) were grounded previously before mixing with the oxalate and FeTMPPCl. This molar ratio of sulfur to metal was previously found to give the best results in terms of activity improvement and removal of inorganic metal species.[14]
These precursors were used for the preparation of the standard catalysts and the catalysts with intermediate acid-leaching. In addition, to elucidate the processes involved in catalyst formation, small quantities of these mixtures were used for the in-situ investigation of the heat-treatment process (HT-XRD and TG-MS measurements).
Preparation of the standard catalysts (± S) Each precursor was filled in a quartz boat, placed in a quartz glass tube and heated from room temperature to 800°C. The heating rate was 7.5 °C/min. At 450°C the samples were held for 10 min before they were heated to 800°C and held at this temperature for 45 min. The complete heat-treatment process was performed in nitrogen atmosphere. After quenching to room temperature (RT), the sample was transferred into 1 M hydrochloric acid and stirred for at least 1 h in an ultrasonic bath. The catalyst was filtrated and washed with distilled water until the filtrate exhibited a pH value of 5. The obtained black catalyst powder was dried at 80 °C. The final catalysts prepared by the pyrolysis of FeTMPPCl and iron-oxalate dihydrate without or with sulfur-addition will be addressed "Fe/Fe–S" and "Fe/Fe+S", respectively.
In a similar way catalysts were prepared by the oxalate-supported pyrolysis of H_2TMPP, utilizing the same molar ratios as given above. These catalysts are labelled "H_2/Fe–S" and "H_2/Fe+S".
Preparation of the reference catalysts (Fe/KB600) The electrochemical bahavior of the prepared catalysts was compared to an impregnation catalyst. The detailed preparation is described in Koslowski et al. (Ref. 8). In short, FeTMPPCl was impregnated on Ketjen Black 600 and subjected to a heating process with 800 °C as end temperature (5 °C/min) followed by a subsequent acid-leaching similar to that of the catalysts prepared by the standard preparation technique. This catalyst is labelled as "Fe/KB600".
Preparation of catalysts with intermediate acid-leaching (± S) In order to verify the findings related to the role of iron-carbide formation during the preparation process, the standard preparation was modified. The precursor mixtures remained the same as for the standard catalysts, but a treatment in an acidic solution as an intermediate step was added.
Each precursor was filled in a quartz boat, placed in a quartz glass tube and heated from room temperature to 500°C (30 min), in a first step. After cooling-down the samples were acid-leached in 1M HCl, similar to the procedure described above. After drying of the intermediates, these were filled again into a quartz boat and heated from room temperature to 800°C, were the temperature was kept for 30 min. After cooling-down to room temperature (RT), again the samples were acid-leaching. Both heat-treatment steps were performed in nitrogen atmosphere with a heating rate of 7.5 °C/min. As the main difference in comparison to the standard preparation is the intermediate acid-leaching, these catalysts are labelled "Fe/Fe–S+IAL" and "Fe/Fe+S+IAL".

II. In-situ characterization of the pyrolysis process

In-situ High-temperature X-ray diffraction measurements (HT-XRD) In order to analyse the solid products that are formed during the heating process, *in-situ* X-ray diffraction measurements were performed at the BESSY II beam line KMC-2 using a stainless-steel reaction chamber with Kapton® windows at the beam entry and exit slits. The precursor samples were placed on an electric graphite heater encapsulated in pyrolytic boron nitride (pBN) from Tectra GmbH. This newly developed reaction chamber is shown in Figure 1 and allows measurements under constant Ar gas flow at reduced pressures in a temperature range from RT to 800 °C applying a heating rate of 7.5 K min^{-1}.[19] A two dimensional detector array (HiStar – Bruker AXS) was used to record the spectra.
Detector, sample and synchrotron-radiation beam were aligned to meet Bragg-Brentano geometry. To simulate the heating process, measurements were carried out under constant Ar flow of 200 ml/min at reduced pressure of p = 400 mbar. As X-ray source synchrotron radiation with energy of 8.731 keV was applied. Calibration of the system was performed using an alumina standard. Because of the reduced pressure, the precursor samples were pelletized (Ø: 10 mm) before placing onto the pBN heating table.
For easier comparison to the X-ray diffractograms of the standard catalysts, the 2θ-values of the XRD peak positions measured with different X-ray sources were referred and compared with those taken at the wavelength of a Cu K_α X-ray tube as shown in the Figures 2c, d and S2.

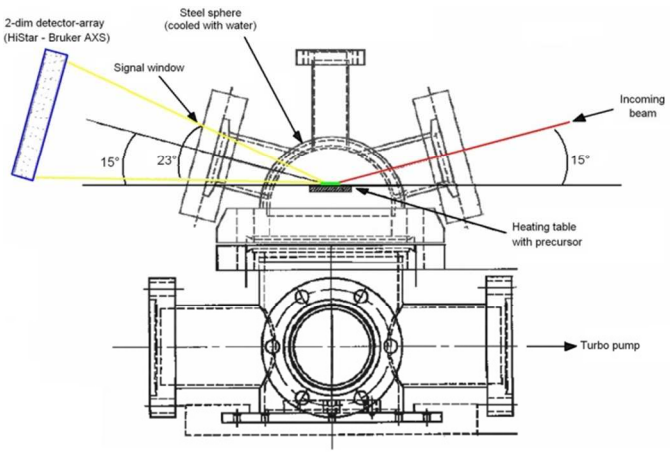

Fig. 1 Reaction chamber for high-temperature X-ray diffraction measurements as performed at the KMC-2 beamline at BESSY II.

Thermogravimetry coupled with mass-spectroscopy (TG-MS) Thermogravimetric measurements were carried out at the Institut für Kristallzüchtung (IKZ) using a NETZSCH Simultaneous Thermal Analyzer STA 409C coupled with a quadrupole mass spectrometer via a skimmer. The measurements were

performed in an Al_2O_3 sample crucible under continuous flow of helium with a heating rate of 7.5 K/min.

III. Characterization of the final catalysts

Electrochemical Characterization Catalyst inks have been prepared by suspending 2 mg of catalyst (Fe/Fe or Fe/Fe/S) in 400 µl of a 1:1 water-ethanol mixture containing 0.2 % Nafion. 5 µl of this suspension were dropped onto a 0.1963 cm^2 glassy carbon disk (RDE) obtaining a catalyst load of 0.13 mg/cm^2. The experiments were carried out at room temperature in a three-electrode-system with a platinum wire as counter electrode and $Hg/Hg_2SO_4/0.5M$ H_2SO_4 as reference electrode (0.68 V vs. SHE).
Prior to the determination of the oxygen reduction current the working electrode with our catalyst was cycled in a potential range from 1.0V to 0.0V with a scan rate of 50 mV/s in nitrogen-saturated 0.5 M H_2SO_4. Typically 15-20 scans were required until a steady state was reached. In the CV diagrams of Figures 4a and 5a always the last scans out of this line are displayed. Previous to the RDE experiments, the electrolyte was purged with oxygen and the open circuit potential (OCP) was measured. RDE experiments were performed with a sweep rate of 5 mV/s in oxygen-saturated electrolyte at 200, 400, 576, 729 and 900 rpm (in this sequence). During the measurement, oxygen was only passed over the surface of the electrolyte. Tafel-plots have been calculated by the Levich-approach. All potentials are given in reference to the standard hydrogen electrode (SHE).
Elemental Analysis In order to determine the elemental composition of the catalysts neutron activation analysis (NAA) and combustion analysis were made to determine the iron contents and the mass-related contents of carbon, nitrogen, sulfur and hydrogen, respectively.
X-ray diffraction For the identification of crystalline phases, XRD measurements of all standard catalysts were carried out employing a Bruker diffractometer D8 Advance in Bragg-Brentano θ-2θ coupling using Cu K_α radiation (λ = 1.54 Å) and a silicon disk as sample holder. Samples were rotated during the measurements. Spectra were recorded in a range of 15° < 2Θ < 60°. The measured diffractograms were analyzed using the database of the Joint Committee on Powder Diffraction Standards (JCPDS).
Raman spectroscopy To characterize the carbon structure, Raman measurements were performed in a range from 1750 to 800 cm^{-1} using a He/Ne laser for the excitation. The catalyst powders were suspended in water and small amounts of these suspensions were dropped onto glass substrates and left to dry. By these treatments flat films of the catalyst powders were obtained on which the laser beam was focused with the help of an optical microscope (Olympus BX). In order to separate Raman and Rayleigh scattering a notch filter and a monochromator were utilized. Raman bands were detected with a CCD camera. For each sample measurements were performed in two different sample areas and the sum spectra were analyzed. Following the semi-empirical equation by Tuinstra and König[20], the graphene layer extensions were calculated:
$L_a = I_{D\text{-}peak}/I_{G\text{-}peak} \cdot 4.4$ nm

^{57}Fe Mößbauer spectroscopy Mößbauer measurements were made to characterize the iron compounds within each standard catalyst. The spectra was recorded at room temperature with a CMCA-550 (Wissel) equipped with a constant electronic drive system with a triangular reference waveform (Halder Electronics). A ^{57}Co/Rh-source was used, velocity scale and isomer shift δ_{iso} were calibrated with natural iron (α-Fe-foil, 25 µm thick, 99.99% purity). An Assignment of the iron species was made by a comparison of the Mößbauer parameters to literature data.

Results

1. Analysis of the pyrolysis process

In order to investigate the pyrolysis process thermogravimetry coupled with mass-spectroscopy (TG-MS) and high-temperature X-ray diffractometry (HT-XRD) were performed for the FeTMPPCl + iron oxalate dihydrate precursor with and without sulfur-addition. In our previous work, TG-MS measurements of different CoTMPP-oxalate precursors have been already described.[6,7] Therefore, only the major differences induced by the addition of sulfur are summarized here, while in the Supplementary Information the TG-MS results are discussed in detail, see Figure S1.
First of all, for both precursors the pyrolysis process can be divided into four sections separated from each other by the release of characteristic gas species. Up to 500°C the thermogravimetric curves appeared to be quite similar. However,

(i) above 500°C the third (and final) decomposition step was shifted from 550°C (as obtained for the sulfur-free precursor) to 750°C for the sulfur-added precursor (see TG-part of Figure S1).

(ii) Due to sulfur-addition, a strong release gaseous sulfur species detected as positively charged fragments in the mass spectrometer were found in the temperature range from 300 to 700°C (m/e = 64 in Figure S1).

(iii) The mass-fragments related to the decomposition of MeN_4-centers (HCN, N_2) showed a single peak for the sulfur-containing precursor (450-520 °C), whereas an additional decomposition peak was observed between 550-650°C for the sulfur-free precursor (m/e = 27, 28 in Figure S1).

The *in-situ* HT-XRD measurements shown in Figure 2 approve that these differences are basically due to the formation of different intermediates during the heating process. Figures 2a and b show the overview of the measurements obtained at temperatures between RT and 800 °C for both precursors. The four different temperature ranges are indicated by roman letters. Note, caused by a thermal-induced expansion of the crystalline phases at higher temperatures the reflexes are shifted to smaller 2θ-angles.

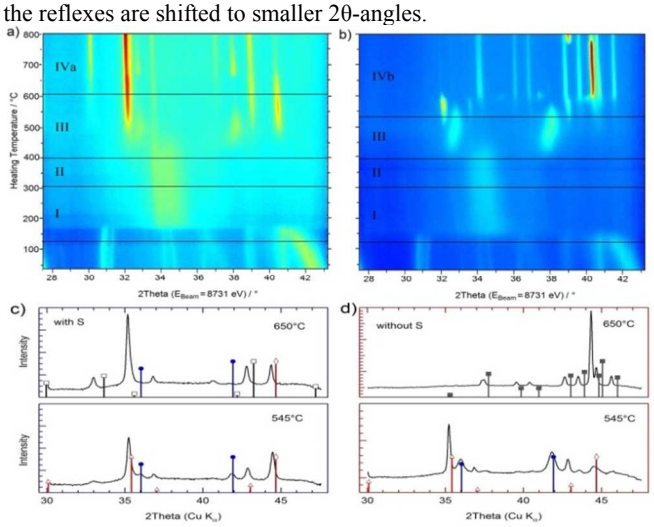

Fig. 2: HT-XRD measurements of the FeTMPPCl + iron oxalate dihydrate precursor mixture with sulfur (a, c) and without sulfur (b, d). Dark blue color denotes low intensity regions and the continuous change to red color indicates an increase of the signal intensity. In c) and d) the X-ray diffractograms as obtained at 545°C and 650°C are extracted. Diffraction patterns can be assigned to troilite FeS (□), wüstite FeO (•), alpha iron (◊), magnetite (Δ), and cohenite Fe_3C (■).

In the Supplementary Information (Figure S2) the extracted diffractograms are given for several temperatures that are representative for the heating processes (usually before and after a main decomposition step). Due to the high amount of iron oxalate dihydrate in the precursor mixture compared to the quantity of porphyrin the diffractogram of the starting material (RT) is dominated by the diffraction reflexes of the oxalate. In agreement with the TG-MS measurements the HT-XRD are similar up to a heat-treatment temperature of 500 °C. Going from the temperature regime I to II (150°C – 200°C) the iron-oxalate dihydrate releases its crystal water and the characteristic diffraction patterns of iron oxalate are found at T > 200°C. In agreement with the thermogravimetric measurements iron oxalate starts to decompose at ca. 400 °C and forms iron-oxide phases (wuestite and magnetite) which can be identified by the diffraction patterns at 435 °C and even more pronounced at 545 °C (see Figures 2c and d). From previous investigations it is known that in the range from 400 to 450°C also the carbonization of the porphyrin precursor is initiated.[5-7,21] In the temperature range 545 °C to 650 °C the reduction of the oxides begins initiated by the in-situ formed carbon. This temperature range seems the most important one related to the changes observed for both final catalysts. Therefore, the XRD diffractograms of both precursors are given after heating to 545 and 650°C in Figure 2c and d, respectively. For the sulfur-free precursor (Fig. 2d), at 650 °C the formation of iron carbide (cohenite) as a reaction product became dominant caused by the reduction of iron oxides formed in the temperature region before.

$$3\ FeO + C \rightarrow Fe_3C + 3/2\ O_2$$

It is important to note, that this is the same temperature range where the additional release of HCN (545 °C – 650 °C) was found (compare main difference (iii)) in TG-MS as discussed above). Between 680 °C and 800 °C the intensity ratio of the cohenite reflexes varies indicating a change in crystal structure.[22]
In contrast to the precursor mixture without sulfur, the carbide formation in the sulfur-containing precursor is inhibited, as can be seen in Figure 2c. The main phases found in the diffractograms are troilite (FeS) and wüstite (FeO). Apparently, sulfur reacts with the formed iron compounds to iron sulfide and suppresses the formation of iron carbide. We will come back to this observation in the discussion part.
In a standard preparation route, the so gained pyrolysis products were conditioned in a subsequent acid-leaching (1 h under ultrasonic treatment in 1 M HCl at 25 °C) in order to remove inactive by-products.

2. Influence of the sulfur-addition on the structural composition of the final catalysts

The X-ray diffractograms, Raman and Mößbauer spectroscopic measurements of the final conditioned catalysts (after pyrolysis (800°C), acid-leaching and washing, compare experimental section) are given in Figure 3 for the FeTMPPCl-related catalysts. In the Supplementary Information, Figure S3, the physical characterizations of the H_2/Fe±S catalysts are shown.
From XRD and Mößbauer measurements of the Fe/Fe-S and H_2/Fe-S catalysts graphite, elemental iron and cohenite can be identified. Apparently, without sulfur-addition the formed iron by-products are hardly accessible during the acid-leaching. As can be seen in Figure S4 for the Fe/Fe-S catalysts these particles are covered by some graphene layers that protect them against the acid attack.
In accord with the XRD data the Raman measurements (Figures 3b, S3b) visualize a higher degree of graphitization of the sulfur-free catalysts (Fe/Fe–S and H_2/Fe–S) as indicated by the higher intensity and smaller full-width at half-maximum of the G-band (and D-band) in comparison to the sulfur-containing catalysts (Fe/Fe+S and H_2/Fe+S). The extensions of the graphene-layers, as calculated from the ratio of D-to-G-peak intensities, are higher for the sulfur-containing catalysts. The diffractograms of the sulfur-added catalysts exhibit predominantly X-ray amorphous behaviour indicating the good solubility of all crystalline iron phases (basically troilite) in acid that were formed until the end of the heat-treatment step.

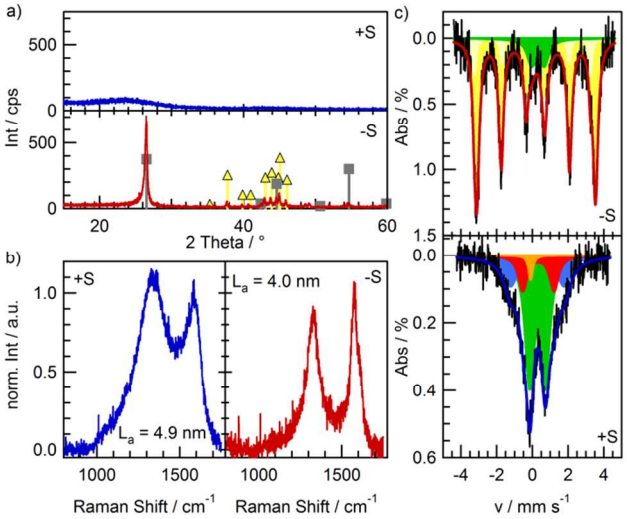

Fig. 3. X-ray diffraction (a), Raman measurements (b) and Mößbauer spectra of the final Fe/Fe-S and Fe/Fe+S catalysts after a pyrolysis up to 800 °C followed by a subsequent acid leaching are given. Diffraction patterns can be assigned to cohenite Fe_3C (Δ), and graphite (■). The Mößbauer parameters and assignment to iron species are summarized in Table S2 in the Supplementary Information.

Table 1 Summary of the atomic concentrations calc. from NAA and combustion analysis. The mass-related concentration of oxygen was first calculated assuming it as difference to 100 wt%. The error is < 10 % for all elements except hydrogen (error bar 10-20 %).

at%	Fe	N	C	H	S	O	ratio N/Fe
Fe/Fe+S	0.66	3.57	70.62	11.89	0.94	12.31	5.4
H_2/Fe+S	0.66	4.11	75.85	6.30	1.84	11.24	6.2
Fe/Fe-S	1.95	0.91	84.4	6.91	0.16	3.95	0.5
H_2/Fe-S	1.71	1.17	78.5	9.23	0.13	9.28	0.7
Fe/KB600	0.22	1.28	92.67	2.1	0.17	3.52	5.8

In Table 1 the results of the chemical composition from bulk-elemental analysis of the catalysts and their [N]/[Fe] ratios are summarized. In agreement with the XRD results the sulfur-free preparation results in a high amount of residual iron whereas the preparation approaches with sulfur lead to low iron concentrations. In contrast, the amount of nitrogen is drastically lower for the sulfur-free catalysts compared to the sulfur-added ones although it was the same in all precursor mixtures (only the porphyrin worked as nitrogen source).
It is important to note, that indicated by a ratio of [N]/[Fe] > 4 the overall iron could be present in FeN_4-centers for both sulfur-added catalyst. From Mößbauer spectroscopy it can be deduced that there is a small contribution of superparamagnetic iron (yellow singlet) can be inferred, what means that iron is not exclusively present in FeN_4-centers. In contrast, the number of FeN_4-centers in the sulfur-free catalysts is limited by their low nitrogen concentrations. In best case,

only a third of the number of active sites compared to the sulfur-containing catalysts has been formed.

3. Effect of sulfur on the electrochemical performance of the final catalysts

Figure 4 gives the cyclic voltammograms (a) and kinetic current density calculated from Levich analysis (b) as a function of the applied potential for both sample series (Fe/Fe ±S and H_2/Fe ±S). It can easily be recognized that the capacity is larger for both sulfur-added catalysts in comparison to the sulfur-free preparations. Furthermore, induced by sulfur-addition more than a 10fold higher kinetic current density was reached and the onset potential (defined as U at -0.05 mA/cm², see Figure S5 for RDE measurements) was shifted from 0.69V to 0.79V and from 0.71V to 0.79V, respectively, for the Fe/Fe and H_2/Fe catalysts.
As a reference, the electrochemical data of Fe/KB600 prepared at the same heat-treatment temperature are additionally shown in Figure 4 (see experimental part for details of its preparation). The kinetic current density of this catalyst (which is free of sulfur) is from the same order of magnitude as the sulfur-added catalysts. For that reason, the high activities of Fe/Fe+S and H_2/Fe+S catalysts are not due to the sulfur-addition but the addition of sulfur prevents a negative effect that appears without it. (Please note: The catalysts prepared by the oxalate-supported pyrolysis can easily be enhanced by subsequent heat-treatment steps to achieve current densities of 9 mA/cm² (at 0.8V).[18] However, a second heat-treatment of the reference catalyst in either N_2 or NH_3 atmosphere led only to a factor of 1.5 higher current densities, compare Figure S6.)

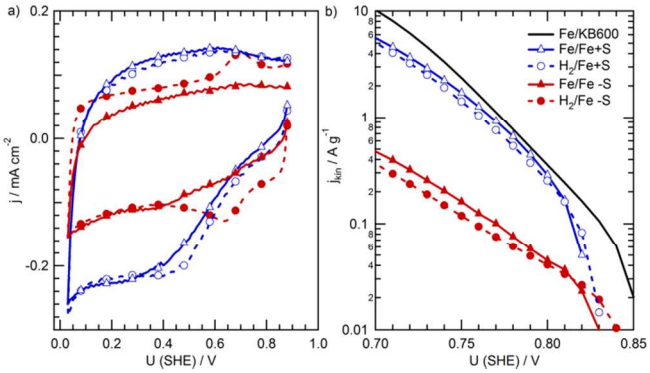

Fig 4. Cyclic Voltammograms (a) and Tafel-plots (b) of the catalysts prepared without and with sulfur in the precursor mixtures.

To further support this argument, the results of bulk-elemental analysis of this reference catalyst are added in Table 1. As iron and nitrogen (from the porphyrin) are only present on the surface of the carbon support the overall concentrations of both elements are smaller compared to the other catalysts. The ratio [N]/[Fe]; however, is similar to both catalysts prepared by adding sulfur to the precursor mixture.

Discussion

1. Role of sulfur during the pyrolysis process

We have seen that on the one hand similar to the CoTMPP-based system also for the oxalate-supported pyrolysis in the presence of FeTMPPCl or H_2TMPP an improved performance can be recognized when the precursors are prepared with sulfur-addition. On the other hand, the comparison to the impregnation catalyst Fe/KB600 prepared by impregnation of a carbon black indicates that the higher catalytic activities of Fe/Fe+S and H_2/Fe+S are not related to an improving effect by the addition of sulfur.
It is well-known that iron catalyses the formation of graphite during high-temperature treatments.[23] In a first step, an amorphous carbon is dissolved in iron or iron-carbide particles. When the solvent gets supersaturated or is quenched, this carbon is precipitated as graphite.[24] The iron is understood as a transport medium whereas the change in free energy from disordered carbon to graphitic carbon is the driving force.[24] Hence, it can be concluded that the neighboured carbon planes (with the integrated catalytic FeN_4-centers) are somehow captured by the iron particles that are formed as final product of the iron oxalate's decomposition under reducing atmosphere (because of the carbon from the porphyrins).
When sulfur is added to the precursor mixture sulfur adsorbs on the iron particles (and iron sulfide is formed during the heat-treatment). Consequently, the agent responsible for the graphitization cannot be formed so that the graphite forming process is inhibited, as described in literature.[25] As a consequence a larger number of catalytic sites remains intact. As no continuous release of HCN-fragments appears (related to the decomposition of active sites) the main FeN_4-decomposition must be assigned to the formation process of iron carbide itself. Since troilite reveals a good solubility in HCl this inactive by-product can easily be removed by the final acid-leaching.[26]

2. Effect of sulfur on the ORR activity

Related to the results in Table 1 and the discussion of the pyrolysis process it can be concluded that without sulfur-addition a higher amount of active sites (FeN_4) are destroyed during the initial iron-carbide formation leading to a smaller ORR current density.
However, comparing the Mößbauer results and the results from bulk-elemental analysis in Table 1 of sulfur-free and sulfur-added catalysts, it becomes clear that the increase in kinetic current density is much higher than the increase in the number of active FeN_4-centers. A direct contribution of sulfur in gaining ORR activity can be excluded as second heat-treatments of the Fe/Fe+S catalysts in ammonia or forming gas lead to a complete removal of sulfur without having a negative effect on the ORR activity. Three different effects might cause the disproportionate increase of kinetic current density:
(1) The formation of iron sulfide in the pyrolysis of the sulfur-added samples leads to an amorphous carbon (see XRD in Figures 3 and S3), that enables a higher electrochemical active surface area (Figure 4a). Hence, a larger number of FeN_4-centers might be accessible during ORR.
(2) The higher doping of the carbon with nitrogen-heteroatoms (estimated from Table 1) could promote the oxygen reduction reaction and enable a higher turn-over frequency (TOF) of the sulfur-added catalysts, as suggested by theoretical calculations and heat-treated carbon-supported FeTMPPCl-based catalysts.[13, 27]
(3) The larger graphene-layer extensions could enable an improved electronic environment that allows a faster ORR (higher TOF).[14]

3. Avoidance of carbide-formation by performing an intermediate acid-leaching

From Figures 2 and S1 it is clear that iron-carbide formation and the disintegration of active sites takes place at temperatures > 550 °C if an excess of iron is present in the precursor mixture. Therefore, an alternative preparation route to prevent the decomposition of FeN_4-centers induced by iron-carbide formation should be the interruption of the pyrolysis process after reaching the temperature of 500°C (see the Experimental part for the details of this preparation).
The performance of an intermediate acid-leaching after quenching of the sample from 500°C to RT for the removal of excess iron should

enable to minimizing carbide formation in the further consecutive heat-treatment process. We tried this variation of the standard oxalate-supported pyrolysis of FeTMPPCl (catalysts have the addition of +IAL (intermediate acid-leaching) to their label). As can be seen from the electrochemical data in Figure 5, these catalysts exhibit indeed similar catalytic performance compared with the sulfur-containing standard catalyst. Therefore, the interruption of the pyrolysis process with an IAL also allows obtaining similar high current densities as with catalysts prepared under sulfur-addition.

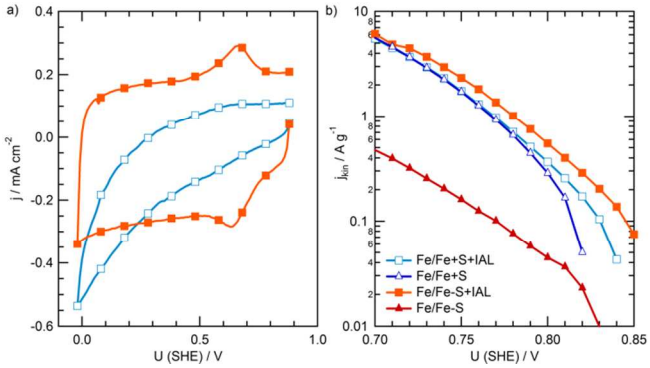

Fig. 5: Cyclic Voltammograms of the catalysts prepared by the oxalate-supported pyrolysis of FeTMPPCl with intermediate acid-leaching (+IAL) (a) and comparison of the Tafel plots of the catalysts obtained by the standard method and the modified preparation route.

With view to literature and the structural characterization of Fe-N-C catalysts discussed in those works, it becomes clear, that most of the catalysts (especially when prepared at higher temperatures) are characterized by the presence of iron carbide.[3,28-32] Hence, we believe that (i) with the optimized addition of sulfur to the precursor mixture in the preparation processes or (ii) by performing an intermediate acid-leaching several catalysts can be enhanced in terms of concentration of active sites and ORR activity.
As sulfur residuals could work as poison during FC run, especially this second approach might be of interest for the preparation of well-performing catalysts.

Conclusions

The oxalate-supported pyrolysis of FeTMPPCl or H_2TMPP enables the preparation of highly active ORR catalysts. On the basis of in-situ High-temperature X-ray diffraction (HT-XRD) and Thermo-gravimetry coupled with mass-spectroscopy (TG-MS) the reasons for the better performance of sulfur-added catalysts was elucidated. The sulfur has no beneficial effect by itself, but it prevents iron-carbide formation during the heating process. As shown by the combination of HT-XRD and TG-MS, the formation of iron carbide causes a disintegration of FeN_4-centers that are known to be responsible for the ORR activity of these Fe-N-C catalysts. Structural characterization of the final catalysts confirms the much lower concentration of FeN_4-centers in the catalysts prepared without sulfur-addition.
On the basis of the performed characterization two options for the enhancement of active site densities of Fe-N-C catalysts can be derived:
(1) Addition of sulfur to the precursor mixture.
(2) Performance of an intermediate acid-leaching to remove excess iron.
As iron carbide is often found as by-product in the preparation of Fe-N-C-catalysts via different approaches we believe that our results have a large impact on the optimization of active site densities (and thus performance) of these catalysts.

Acknowledgements

TG-MS measurements were performed at the Institut für Kristallzüchtung IKZ with the help of Dr. Klimm. Sven Kubala (now FHI) was of great support for his substantial contribution in adapting the HT-XRD measuring cell to the harsh in-situ reaction environment. Bulk-elemental analysis and NAA were performed by Prof. Linker and Dr. Alber, respectively. Mößbauer spectroscopy was performed with the help of Prof. em. Abs-Wurmbach at the Institute of Technology Berlin. Their help for the fruitful development of these data is greatfully acknowledged. Furthermore, we would like to thank the BESSY team for the comprehensive technical support during beam time.

Notes and references

[a] Helmholtz-Centre Berlin for Materials and Energy, Institute of Solar Fuels, Hahn-Meitner-Platz 1, 14109 Berlin, Germany
[b] Brandenburgische Technische Universität Cottbus-Senftenberg, Chair of Applied Physics and Sensors, Konrad-Wachsmann-Allee 17, 03046 Cottbus, Germany; * E-mail: kramm@tu-cottbus.de, Tel. +49-355-69-2972
[c] Helmholtz-Centre Berlin for Materials and Energy, BESSY II, Albert-Einstein-Str. 15, 12489 Berlin, Germany

Electronic Supplementary Information (ESI) available: [Detailed discussion of the pyrolysis process of the FeTMPPCl+iron-oxalate-dihydrate precusors with and without sulfur by TG-MS and selected diffractograms of HT-XRD measurements; Physical characterization of the H_2/Fe+S and H_2/Fe-S catalysts (by XRD, Raman spectroscopy and Mößbauer spectroscopy); Table summarizing the Mößbauer parameters and assignments to iron species of all standard catalysts; TEM images of Fe/Fe-S catalyst; RDE measurements with rpm200, 400, and 900 of all standard catalysts. Comparison of the effect of a second heat-treatment in either N_2 or NH_3, respectively, on the ORR activity of the reference catalyst and Fe/Fe+S.] See DOI: 10.1039/b000000x/

1 A. de Frank Bruijn and G.J.M. Janssen in E*ncyclopedia of Sustainable Science and Technology*; Meyers, R. A., Ed.; Springer NY: 2013, 7694.
2 M. Lefèvre, E. Proietti, F. Jaouen and J.-P. Dodelet, *Science* 2009, **324**, 71.
3 E. Proietti, F. Jaouen, M. Lefèvre, N. Larouche, J. Tian, J. Herranz and J.-P. Dodelet, *Nature Comm.* 2011, **2**, 416.
4 G. Wu, K.L. More, C.M. Johnston and P. Zelenay, *Science* 2011, **332**, 443.
5 P. Bogdanoff, I. Herrmann, M. Hilgendorff, I. Dorbandt, S. Fiechter and H. Tributsch, *J. New. Mat. Electrochem. Systems* 2004, **7**, 85.
6 I. Herrmann, U.I. Kramm, S. Fiechter and P. Bogdanoff, *Electrochim. Acta* 2009, **54**, 4275.
7 I. Herrmann, U.I. Kramm, J. Radnik, P. Bogdanoff and S. Fiechter, *J. Electrochem. Soc.* 2009, **156**, B1283.
8 U.I. Koslowski, I. Abs-Wurmbach, S. Fiechter and P. Bogdanoff, *J. Phys. Chem. C* 2008, **112**, 15356.
9 U.I. Kramm, I. Herrmann-Geppert, P. Bogdanoff, and S. Fiechter, *J. Phys. Chem. C* 2011, **115**, 23417.
10 H. Tributsch, U.I. Koslowski and I. Dorbandt, *Electrochim. Acta* 2008, **53**, 2198.
11 U.I. Koslowski, I. Herrmann, P. Bogdanoff, C. Barkschat, S. Fiechter, N. Iwata, H. Takahashi and H. Nishikoro, *ECS Trans.* 2008, **13**, 125.

12 U.I. Kramm, I. Herrmann, S. Fiechter, G. Zehl, I. Zizak, I. Abs-Wurmbach, J. Radnik, I. Dorbandt and P. Bogdanoff, *ECS Trans.* 2009, **25**, 659.
13 U.I. Kramm, I. Abs-Wurmbach, I. Herrmann-Geppert, J. Radnik, S. Fiechter and P. Bogdanoff, *J. Electrochem. Soc.* 2011, **158**, B69.
14 I. Herrmann, PhD Thesis, Freie Universität Berlin, 2006.
15 M. Ferrandon, A.J. Kropf, D.J. Myers, K. Artyushkova, U.I. Kramm, P. Bogdanoff, G. Wu, C.M. Johnston and P. Zelenay, *J. Phys. Chem. C* 2012, **116**, 16001.
16 O. Contamin, C. Debiemme-Chouvy, M. Savy and G. Scarbeck, *Electrochim. Acta* 1999, **45**, 721.
17 T.D. Hatchard, J.E. Harlow, K.M. Cullen, R.A. Dunlap, J.R. Dahn, *J. Electrochem. Soc.* 2010, **159**, B121.
18 F. Jaouen, J. Herranz, M. Lefèvre, J.-P. Dodelet, U.I. Kramm, I. Herrmann, P. Bogdanoff, J. Maruyama, T. Nagaoka, A. Garsuch, J.R. Dahn, T.S. Olson, S. Pylypenko, P. Atanassov and E.A. Ustinov, *Appl. Mater. Interf.* 2009, **1**, 1623.
19 U.I. Kramm, G. Zehl, I. Zizak, I. Herrmann, I. Dorbandt, P. Bogdanoff and S. Fiechter, *Bessy Annual Report* 2008, 39-41.
20 F. Tuinstra and J.L.König, *J. Chem. Phys.*, 1970, **53**, 1126.
21 I. Herrmann, U.I. Kramm, S. Fiechter, V. Brüser, H. Kersten and P. Bogdanoff, *Plasma Process. & Polym.* 2010, **7**, 515.
22 A.F. Holleman, and E. Wiberg, E. *Lehrbuch anorg. Chem.*; Walter de Gruyter & Co: Berlin, 1960; Vol. **47-56**.
23 K. Kinoshita, *Carbon – Electrochem. Physicochem. Properties*; Wiley-Interscience; 1st edition, 1987.
24 H. Marsh, and A.P. Warburton, *J. Appl. Chem.* 1970, **20**, 133.
25 H.J. Grabke, D. Moszynski, E.M. Müller-Lorenz, and A. Schneider, *Surf. Interf. Analysis* 2002, **34**, 369.
26 P. Ramdohr and H. Strunz, *Klockmanns Lehrbuch der Mineralogie*; Ernst Klett Verlag: Stuttgart, 1978/1980; Vol. **16**.
27 V.V. Strelko, V.S. Kuts and P.A. Thrower, *Carbon* 2000, **38**, 1499.
28 A. Garsuch, R. d'Eon, T. Dahn, O. Klepel, R.R. Garsuch and J.R. Dahn, *J. Electrochem. Soc.* 2008, **155**, B236.
29 G. Liu, X. Li, P. Ganesan and B.N. Popov, *Appl. Catal. B: Environm.* 2009, **93**, 156.
30 S.-H. Liu, and J.-R. Wu, *Microporous and Mesoporous Materials* 2013, **170**, 150.
31 H. Meng, N. Larouche, M. Lefèvre, F. Jaouen, B. Stansfield and J.-P. Dodelet, *Electrochim. Acta* 2010, **55**, 6450.
32 J. Wu, W. Li, D. Higgins and Z. Chen, Z. *J. Phys. Chem. C* 2011, **115**, 18856.